Automated Bridge Deck Evaluation through UAV Derived Point Cloud

Siyuan Chen[1], Linh Truong-Hong[1], Debra F. Laefer[1,2], Eleni Mangina[3]

[1]Department of Civil Engineering, University College Dublin, Ireland

[2]Center for Urban Science and Progress and Department of Civil and Urban, New York University, US

[3]Department of Computer Science, University College Dublin, Ireland

Email : siyuan.chen@ucd.ie, linh.truonghong@ucd.ie, debra.laefer@nyu.edu, eleni.mangina@ucd.ie

ABSTRACT: Imagery-based, three-dimensional (3D) reconstructions from Unmanned Aerial Vehicles (UAVs) hold the potential to provide a safer, more economical, and less disruptive approach for bridge inspection. This paper describes a methodology using a low-cost UAV to generate an imagery-based, dense point cloud for bridge deck inspection. Structure from motion (SfM) is employed to create a three-dimensional (3D) point cloud. Outlier data are removed through a density-based filtering method. Next, the unsupervised learning algorithm k-means and an object-based region growing algorithm are compared for accuracy with respect to bridge deck extraction. Last, an automatic pavement evaluation method is proposed to estimate the deck's pavement condition. The procedure is demonstrated through an actual case study, in which a 3D point cloud of 16 million valid points was generated from 212 images. With that data set, the region growing method successfully extracted the deck area with an F-score close to 95%, while the unsupervised learning approach only achieved 76%. In the last, to evaluate the surface condition of the extracted pavement, a polynomial surface fitting method was designed to evaluate and visualise the damages.

KEYWORDS: UAV, Bridge inspection, Point cloud, Segmentation, Deck Extraction, Pavement Inspection, SfM.

1 INTRODUCTION

Bridge inspection has traditionally been conducted by highly-skilled inspectors but associated with safety problems, especially for those inspectors. While van- and robot-based inspection capabilities have been developed to replace in-person methods [1], ultimately those inspection methods still rely on the physical inspectors or machines on site, which cause traffic closure and/or high equipment costs.

Advances in the unmanned aerial vehicle (UAV) industry and in computer vision have enabled the introduction of low-cost UAVs into the market and affiliate image process techniques that can be paired for bridge documentation. This type of approach is attractive, because it involves non-contact measurement, no traffic closures, no heavy/special equipment, and no need for experienced inspectors on-site. Additionally, the state-of-the-art computer vision-based methods allow generation of accurate, highly dense point clouds from UAVs-images with a single digital camera, which shows UAV-based abilities to capture three-dimensional (3D) topographic data of structures. These new abilities coupled with lower costs have accelerated the adoption of UAVs for infrastructure documentation related tasks including building modelling [2], dam inspection [3], and road surface evaluation [4].

However, most existing UAV work is focused on 3D model generation and does not address the specific aspects related to inspection. To address these gaps, this study first presents a work flow of utilizing a Structure from Motion (SfM) approach to generate a point cloud from low-altitude, aerial images collected by a low–cost UAV. Then, a noise reduction algorithm is introduced. Next a comparison of two deck extraction methods is made (a machine learning clustering method and an object segmentation approach involving a region growing algorithm). Finally a means is provided for automated deck inspection.

2 RELATED WORKS

2.1 UAV Based 3D Reconstruction and Noise Removal

In recent years, less expensive and more easily controllable UAVs have increased their popularity for low altitude, close-range infrastructure inspection [5]. To aid in such activities, a wide range of detectors have been applied, such as digital cameras [6], laser scanners [7], multi-spectral cameras [8] and thermal cameras [9]. Among those, the digital camera is the cheapest and most common. A straightforward approach to achieve documentation with this equipment involves capturing two-dimensional (2D) images for analysis. For example, Chen et al. collected 2D imagery for identifying highway bridge cracks [10]. However, 2D images do not provide depth information directly, which precludes calculating volumetric damage (e.g. spalling). An alternative solution involves using images captured from multiple view angles to reconstruct an object in three dimensions (3D). A common strategy to achieve this is through the application of SfM [11] to multiple images taken from a single camera. SfM has been extensively studied and widely applied for a range of related applications [e.g. 12-14].

In general, SfM detects key (i.e. unique) features from each image. As these images are taken from multiple viewpoints, by linking these key points together, a 3D structure can be assembled (e.g. [15]). Compared to the traditional 3D point cloud generation methods from laser scanning, the UAV imagery reconstructed point offers the opportunity to include data obtained from less restricted by view angles, than from many other means, thereby providing better coverage at lower

costs. However, imagery-based point clouds are often much noisier than those from laser scanning data. Noise typically occurs from structural artefacts in the acquisition process or mismatching of features in images during the reconstruction process [16]. Noisy points can affect further surface reconstruction or point classification for damage detection. To minimize these negative effects, post-processing is applied for noise reduction. A typical solution involves the Statistical outlier removal (SOR) filter, which assumes that noisy points have distinguishable characteristics from non-noisy point in a k-dimensional space when fitting the data to a standard probability distribution [17].

2.2 Possible Bridge Deck Extraction and Evaluation Approaches

The task of bridge deck extraction relies on point cloud segmentation. This can be achieved by numerous means, but two common approaches involve either (1) machine learning or (2) object-based segmentation [18]. While machine learning based clustering can include multiple methods such as k-means, mean shift, neural network, and deep learning, this paper uses the k-means clustering. This method is able to classify 3D points into K groups using different features. The grouping is done by minimizing the sum of squares of distances between the point and the corresponding cluster centroid [19]. In contrast, object-based segmentation can be described as belonging to a class of procedures involving model fitting and region growing methods [20]. The model fitting method uses geometric primitives like planes, cylinders, and spheres to fit the point could and decompose the object. The approach works well for simple structures but tends to perform poorly in the face of large data sets or complex geometries [18]. Thus, this method is not considered further in this study, as the bridge structure is likely be too complex to decompose – a problem previously noted by researchers using laser scans [21, 22]. The region growing method uses local features extracted from a neighbourhood around each point to aggregate nearby points with similar properties and thereby segment a region of a point cloud [20].

However, aforementioned studies have been focused on processing point cloud data derived from laser scanning. Such point clouds differ from those derived from imagery in several import ways. First, the laser scanning data do not contain red-green-blue (RGB) values, unless captured with an integrated camera. Instead, they have affiliated intensity measurements based on the strength of the returning laser signal. Second, the distribution of laser scanning points tends to follow specified patterns based on the pre-programmed operational movements of the scanner. Conversely, the imagery derived points are more randomly distributed around the structure surface, especially when acquired from a UAV, even if the UAV is following a pre-programmed flight path. This difference in data acquisition leads to differences in density and normals.

In the case of a stationary laser scanner, density degradation is more predictable (e.g. if scanning from a river bank, the angle of incidence combined with the offset will impact the point yield, as described in detail in [23] and demonstrated by Truong-Hong in the case of a metal bridge in [24]). As features play important roles in the point cloud segmentation process, there is a need to prioritize finding robust and relevant features

in the derived heterogeneous point cloud. These issues have yet to be addressed systematically in the peer-reviewed literature.

3 WORKFLOW FOR UAV-BASED BRIDGE DECK INSPECTION

To overcome some of these difficulties, a new work flow is proposed, as shown in Figure 1. First, a low-cost, commercial UAV is employed for image acquisition. Then, SfM is applied to generate a 3D point cloud from the 2D images. Next, noise caused by shadows and water reflections are removed automatically with a novel, new algorithm. Then an automatic deck extraction step occurs. Finally, a health evaluation matrix is proposed for deck assessment. Notably, herein two deck extraction approaches are compared: k-means clustering and region growing.
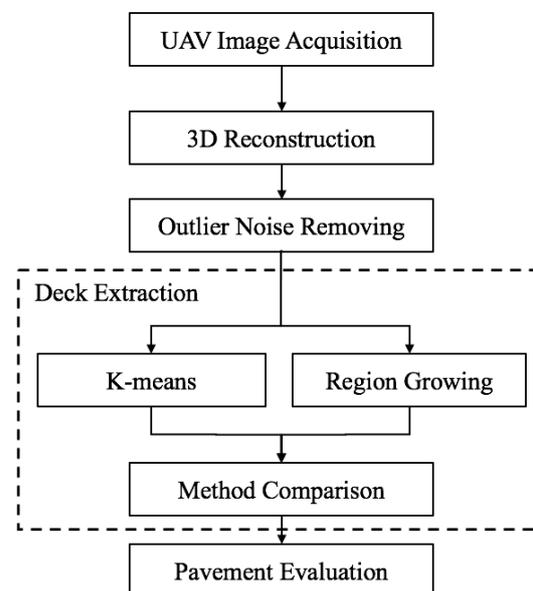
Figure 1. Flowchart of data processing of the developed bridge deck inspection system.

3.1 Image Acquisition

To validate the approach, a case study was conducted using the Blessington bridge in County Wicklow, Ireland. The bridge is of reinforced concrete and about 130 m long, 8 m wide, and situated 10 m above the water (Figure 2). A DJI Phantom 4 quadrotor was equipped with a 4K camera and a 3-axis gimbal; (total cost about 1,500 euros). To ensure full acquisition, 7 parallel flight paths along the bridge were undertaken (2 from each side of the bridge and 3 above the deck). Acquisition occurred from 10 to 20 m away. UAV operations were manually controlled by a remote pilot through a first-person view camera, with a safety inspector in attendance to watch for obstacles (e.g. trees, wires, birds). A total of 212 images were captured in a 1 hour duration.

a.   Aerial image

b. Bridge deck
Figure 2. Blessington bridge

3.2   3D Reconstruction

The 3D reconstruction process was performed in the commercial software PhotoScan [25] on a Dell XPS 15 laptop (i7 CPU with a clock speed 2.8Ghz, 4 cores, 16 Gb RAM, and the Microsoft Windows 10 operating system). The entire reconstruction processing took about 1 hour and generated a point cloud of approximately 16.8 million points (Figure 3). The achieved ground resolution was 8.18 mm/pix. See Table 1 for more details.
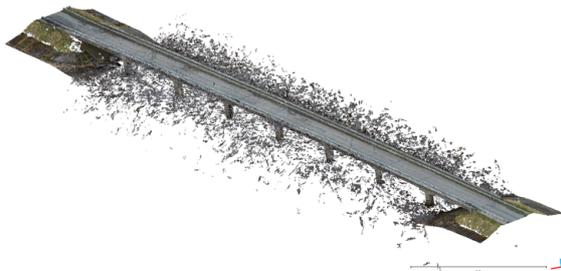
Figure 3. Original point cloud data with significant quantities of noise in evidence

Table 1. 3D Reconstruction Result.

Number of images	212
Ground resolution	8.18 mm/pix
Spare points number	261,442
Spare reconstruction time	34 minutes
Dense points number	16,805,020 points
Dense reconstruction time	31 minutes

3.3   Outlier Noise Removing

Point clouds reconstructed from UAV images tend to be noisy. In this case study, much of noise appeared just beyond the bridge's boundaries, especially under the bridge. This was caused by waves, water reflection, and self-shadows. The noise greatly affects further point cloud processing. Therefore, an automatic denoising approach was devised. This involved calculating the volume density in a spherical neighbourhood of radius R (Figure 4a) for each point. In this case study, R was set to 0.5 m which mast bigger than the regular size of noise clusters. If the density was less than the threshold K, the point was labelled as an outlier. The threshold K was automatically set to equal the average density of the entire dataset minus one standard deviation. In this instance, K equalled 1600 points in the specified neighbourhood.
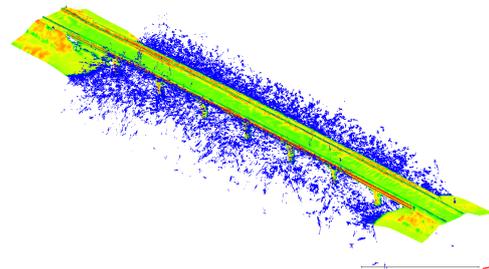
a.   Point density distribution

b.   Point cloud after automatic noise removal

Figure 4. Input data

3.4   Bridge Deck Extraction

As mentioned previously, two methods were compared herein: k-means clustering and region growing. The k-means processing is achieved by the blind-in function in the Matlab software [26]. While, the details of the implemented region growing algorithm can be found in reference [20]. For both methods, features of each point must be calculated prior to the extraction process. In this study, the geometric location (x y z), normal (Nx Ny Nz), colour information (R G B), density (with a searching radius r = 0.25 m), Gaussian curvature (r = 0.25m), and Roughness (r = 0.25m) were calculated within the software CloudCompare [27].

3.5   Extraction Performance Comparison

To evaluate the performance of two extraction methods, three metrics were employed to measure the overall accuracy and effectiveness of a segmentation. They were precision (Eqn 1), recall (Eqn 2) and F-score (Eqn 3). These metrics are based on the following values: (i) True Positives (TP), which represents proper segmentation that matches with a manually generated

ground truth benchmarked by human experts; (ii) False Positives (FP), which denotes over-segmentation within point cloud models that results in segmenting one 'reference' segment into several parts; and (iii) False Negatives (FN), which happens when two or more separate segments are wrongly grouped together leading to under-segmenting the 3D model.

$$Precision = \frac{|TP|}{|TP| + |FP|} \quad (1)$$

$$Recall = \frac{|TP|}{|TP| + |FN|} \quad (2)$$

$$F - score = 2 \times \frac{Precision \times Recall}{Precision + Recall} \quad (3)$$

3.6 Pavement Evaluation

To evaluate the surface condition of the extracted pavement, a second-order polynomial surface (Eqn 4) was generated to fit the dataset to simulate the original pavement surface. Then, for each point P_i, the distance D_i (Eqn 5) from the current surface to the artificial simulated surface was calculated to identify the wear condition of the deck surface.

$$sf(x, y) = P_0 + P_1 \times X + P_2 \times Y + P_3 \times X^2 \quad (4)$$
$$+ P_4 \times Y^2 + P_5 \times X \times Y$$
$$D_i = z_i - sf(x_i, y_i) \quad (5)$$

4 RESULT ANALYSIS

4.1 Extraction Result Analysis

First, the k-means clustering process was applied individually to each of the six sets of feature (see section 3.4). As shown in Table 2 and Figure 5, the result based on the 'normal' had a higher F-score, 0.76. When the normal was paired with other features (Figure 6 and Table 3), the combination of the normal and the z (elevation) produced the best outcome of the combined features. However, the top score 0.75 was slightly less than that produced using only the normal. Thus demonstrating that the presence of more features does not guarantee a more accurate result.

As the results could have been affected by the expected cluster numbers, k, a further test was conducted to segment the dataset into 6, 8, 9, 10 and 12 clusters, as shown in Table 4. Figure 7 shows that the k value does not have a significant effect on the results. However, a higher k value will decrease the recall rate, because of over-segmentation of the deck into small sections resulting in their exclusion from the main cluster.

Table 2. k-means Results with one feature

Features						K	Time		Result	
Normal	Z	RGB	Curvature	Residual	Density		(s)	Precision	Recall	F-score
✔						8	34.7	0.6279	0.9844	0.7667
	✔					8	117.17	0.4876	0.6351	0.5516
		✔				8	161.37	0.7452	0.3025	0.4303
			✔			8	114.19	0.3226	0.9988	0.4877
				✔		8	16.79	0.489	0.3929	0.4357
					✔	8	28.18	0.1446	0.1544	0.1494
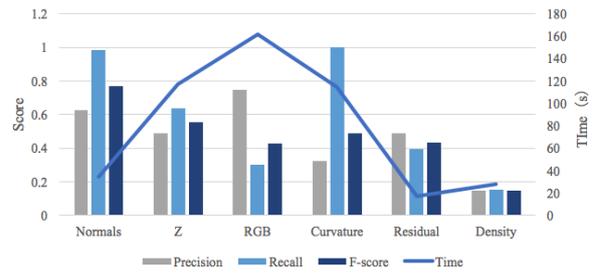
Figure 5. Single feature comparison

Table 3. k-means Result with two features

Features						K	Time		Result	
Normal	Z	RGB	Curvature	Residual	Density		(s)	Precision	Recall	F-score
✔	✔					8	64.37	0.6021	1	0.7516
✔		✔				8	195.56	0.7571	0.389	0.5139
✔			✔			8	150.8	0.391	0.9985	0.562
✔				✔		8	28.51	0.5765	0.4735	0.52
✔					✔	8	66.3	0.6618	0.6051	0.6322
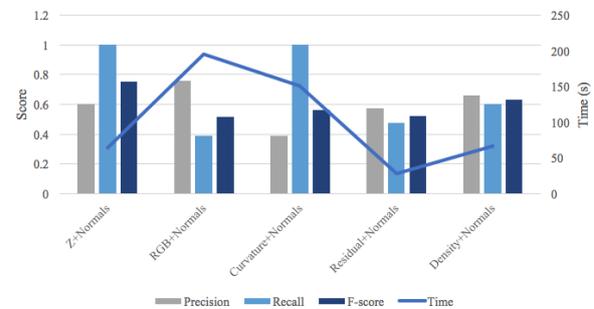
Figure 6. Multiple feature comparison

Table 4. k-means results with different K values when using both the normal and z feature

K	Time		Result	
	(s)	Precision	Recall	F-score
12	149.19	0.5855	0.6612	0.6211
10	186.29	0.5865	0.6752	0.6277
9	168.59	0.5933	1	0.7447
8	64.37	0.6021	1	0.7516
6	102.19	0.5934	1	0.7448
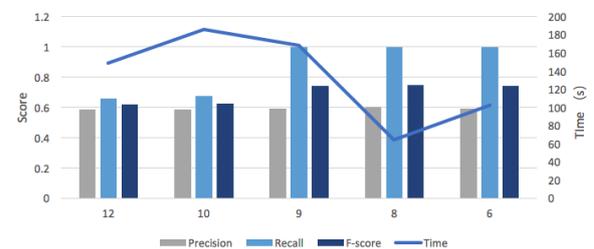
Figure 7. Comparison of different K values

The results of the region growing method are shown in Table 5 and Figure 8. Normal feature, elevation (z), curvature, and residual were applied. The F-score reached 0.94 which was nearly 20% better than achieved by than the k-Means method, (Table 2 vs Table 5).

Table 5. The region growing method result

Time	Precision	Recall	F-score
188.61	0.9177	0.9809	0.9482

a

b
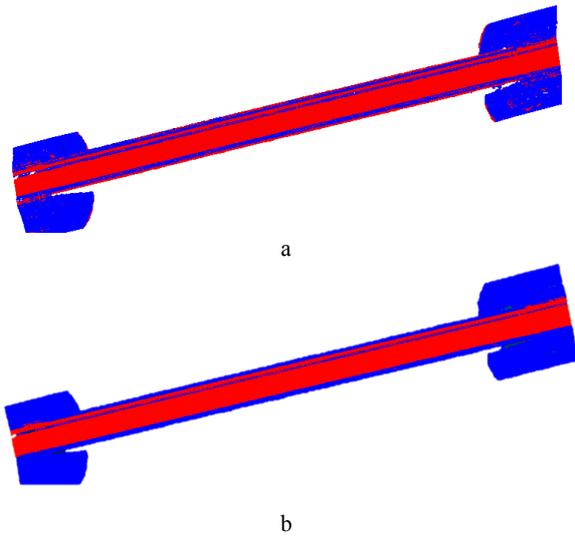
Figure 8. The extraction results a. k-means b. R growing

4.2 Pavement Condition Analysis

The extracted bridge deck was then subjected to the pavement condition approach introduced in section 3.6. The result are shown in Figure 9. The condition map of the extracted pavement shows that the overall damage was heavier in the quarter span location, with small localized damage like potholes or erosions also visible.
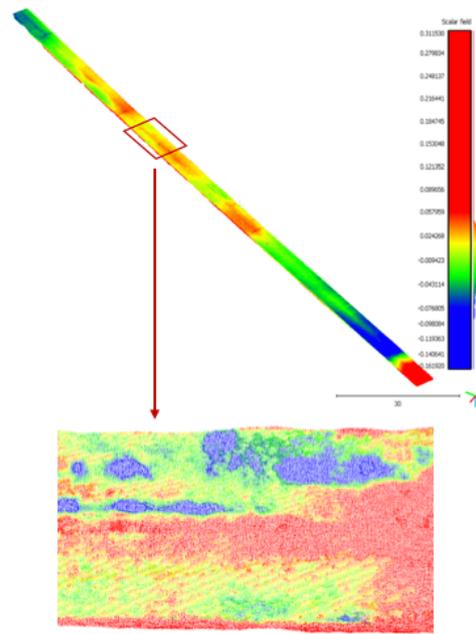
Figure 9. Pavement condition map showing damage and erosion

5 CONCLUSIONS

Using UAV-based imagery, this paper introduces a complete workflow for bridge deck assessment, which involves prior steps of 3D point cloud reconstruction, noise reduction, deck extraction. Importantly, the proposed deck evaluation approach offers an automated means to estimate the surface conditions. This approach can be used for generating the health map as a reference for safety analysis. Additionally two bridge deck segmentation methods (k-means and region growing method) were compared, where the region growing method was able to generate an F-score close to 95% for bridge deck extraction, while the k-means only achieved 76%.

REFERENCES

[1]   H. M. La, N. Gucunski, K. Dana, and S.-H. Kee, "Development of An Autonomous Bridge Deck Inspection Robotic System," *J. F. Robot.*, vol. 2017 Apr 2, no. arXiv:1704.07400v1, pp. 1–25, 2017.

[2]   J. Byrne, E. O'Keeffe, D. Lennon, and D. F. Laefer, "3D Reconstructions Using UnstabilizedVideo Footage from an Unmanned Aerial Vehicle 3D Reconstructions Using Unstabilized Video Footage from an Unmanned Aerial Vehicle," *J. Imaging*, vol. 3, p. 15, 2017.

[3]   N. Hallermann, G. Morgenthal, and V. Rodehorst, "Unmanned Aerial Systems (UAS) – Case Studies of Vision Based Monitoring of Ageing Structures," *Int. Symp. Non-Destructive*, no. September, pp. 15–17, 2015.

[4]   S. Distresses and C. Zhang, "An Unmanned Aerial Vehicle-Based Imaging System for 3D Measurement of Unpaved Road," vol. 27, pp. 118–129, 2012.

[5]   S. Chen, D. F. Laefer, and E. Mangina, "State of Technology Review of Civilian UAVs," *Recent Patents Eng.*, vol. 10 (3) 201, pp. 160–174, 2016.

[6]   H. Kim, J. Lee, E. Ahn, S. Cho, M. Shin, and S. Sim, "Concrete Crack Identification using UAV incorporating Hybrid Image Processing," pp. 1–14, 2017.

[7]   D. Holz, M. Nieuwenhuisen, D. Droeschel, M. Schreiber, and S. Behnke, "Towards Multimodal Omnidirectional Obstacle Detection for Autonomous Unmanned Aerial Vehicles," *Int. Arch. Photogramm. Remote Sens. Spat. Inf. Sci.*, vol. XL-1/W2, no. September, pp. 4–6, 2013.

[8]   X. Zhu, X. Li, and F. Yan, "Design and implementation for integrated UAV multi-spectral inspection system Design and implementation for integrated UAV multi-spectral inspection system," in *Asia Conference on Energy and Environment Engineering*, 2018, p. Vol. 133. No. 1.

[9]   T. Omar and M. L. Nehdi, "Automation in Construction Remote sensing of concrete bridge decks using unmanned aerial vehicle infrared thermography," *Autom. Constr.*, no. June, pp. 1–12, 2017.

[10]   S. Chen, M. Asce, C. Rice, C. Boyle, and E. Hauser, "Small-Format Aerial Photography for Highway-Bridge Monitoring," vol. 25, no. April, pp. 105–112, 2011.

[11]   S. Ullman, "The Interpretation of Structure from Motion," *Proc. R. Soc. London. Ser. B, Biol. Sci.*, vol. 203, no. 1153, pp. 405–426, 1979.

[12]   T. Moons, M. Vergauwen, and L. Van Gool, "3D reconstruction from multiple images," pp. 1–10, 2008.

[13]   S. Agarwal, N. Snavely, I. Simon, S. M. Seitz, and R. Szeliski, "Building rome in a day," *Commun. ACM*, vol. 54, no. 10, pp. 105–112, 2011.

[14]   N. Micheletti, J. H. Chandler, and S. N. Lane, "Structure from Motion (SfM) Photogrammetry," *Br. Soc. Geomorphol. Geomorphol. Tech.*, vol. 2, no. 2, pp. 1–12, 2015.

[15]   J. Byrne, D. F. Laefer, and E. O'Keeffe, "Maximizing feature detection in aerial unmanned aerial vehicle datasets," *J. Appl. Remote Sens.*, vol. 11(2), pp. 1–2, 2017.

[16]   M. Berger, P. Alliez, A. Tagliasacchi, L. M. Seversky, C. T. Silva, J. A. Levine, and A. Sharf, "State of the Art in Surface Reconstruction from Point Clouds," in *EUROGRAPHICS star reports*, 2014, p. Vol. 1, No. 1, 161-185.

[17]   A. Nurunnabi, G. West, and D. Belton, "Outlier detection and robust normal-curvature estimation in mobile laser scanning 3D point cloud data," *Pattern Recognit.*, vol. 48, no. 4, pp. 1404–1419, 2015.

[18]   C. Paper, A. Nguyen, and I. Italiano, "3D point cloud segmentation : A survey 3D Point Cloud Segmentation : A survey," no. November, 2013.

[19]   E. Grilli, F. Menna, F. Remondino, L. Scanning, and L. Scanner, "A REVIEW OF POINT CLOUDS SEGMENTATION AND CLASSIFICATION ALGORITHMS," in *The International Archives of the Photogrammetry, Remote Sensing and Spatial Information Sciences*, 2017, vol. XLII-2/W3, no. March, pp. 339–334.

[20]   A. V. Vo, L. Truong-Hong, D. F. Laefer, and M. Bertolotto, "Octree-based region growing for point cloud segmentation," *ISPRS J. Photogramm. Remote Sens.*, vol. 104, no. October 2016, pp. 88–100, 2015.

[21]   D. F. Laefer and L. Truong-hong, "Automation in Construction Toward automatic generation of 3D steel structures for building information modelling," *Autom. Constr.*, vol. 74, pp. 66–77, 2017.

[22]   D. F. Truong-Hong, Linh; Laefer, "Application of terrestrial laser scanner in bridge inspection: review and an opportunity," in *37th IABSE Symposium: Engineering for Progress, Nature and People*, 2014.

[23]   D. F. Laefer, M. Fitzgerald, E. M. Maloney, D. Coyne, D. Lennon, and S. Morrish, "Lateral image degradation in terrestrial laser scanning Author(s)," *Struct. Eng. Int.*, no. 19 (2), pp. 184–189, 2009.

[24]   N. Gyetvai, L. Truong-Hong, and D. F. Laefer, "Laser scan-based structural assessment of wrought iron bridges : Guinness Bridge, Ireland," *Proc. Inst. Civ. Eng. Hist. Herit.*, vol. 171, pp. 76–89, 2018.

[25]   Agisoft, "Agisoft PhotoScan," 2017.

[26]   Matlab 2018a, "k-means clustering." [Online]. Available: https://uk.mathworks.com/help/stats/kmeans.html.

[27]   CloudCompare, "CloudCompare," *Stereo, V2.9, Open Source Project*, 2017. [Online]. Available: http://www.danielgm.net/cc/.